Supporting Information

N-doped carbon substrate makes Ru-Co alloy an efficient electrocatalyst for pH-universal seawater splitting

*Kang-Yi Xiong,[+a] Le-Wei Shen,[+a] Yong Wang,[+a] Yu Liu,[a] Ming-Xia Hu,[a] Jie Ying,[b] Yu-Xuan Xiao,[b] Ling Shen[*a] Ge Tian[*a] and Xiao-Yu Yang[*a, c]*

[a.] State Key Laboratory of Advanced Technology for Materials Synthesis and Processing, and International School of Materials Science and Engineering, and School of Materials Science and Engineering, and Shenzhen Research Institute, and Laoshan Laboratory, Wuhan University of Technology, Wuhan, Hubei, 430070, China.

Email: *xyyang@whut.edu.cn* (X.Y.Y.); *tiange@whut.edu.cn* (G. T.) *lingshen@whut.edu.cn* (L. S.)

[b.] School of Chemical Engineering and Technology, Sun Yat-sen University, Zhuhai 519082, China.

[c.] National Energy Key Laboratory for New Hydrogen-Ammonia Energy Technologies Foshan Xianhu Laboratory, Foshan 528200, China.

EXPERIMENT SECTION

Chemicals and Materials. All chemicals were analytical grade. Ruthenium (III) chloride hydrate ($RuCl_3 \cdot xH_2O$, 35.0-42.0% Ru basis), cobalt chloride hexahydrate ($CoCl_2 \cdot 6H_2O$), potassium citrate ($C_6H_9KO_7$), Potassium cobalt cyanide ($K_3[Co(CN)_6]_2$), sodium borohydride ($NaBH_4$), potassium hydroxide (KOH), sodium chloride (NaCl), ruthenium(IV) oxide (RuO_2), hydrazine monohydrate (N_2H_4 H_2O), Nafion (5 wt. %), and isopropyl alcohol (C_3H_8O) were purchased from Shanghai Aladdin Biochemical Polytron Technologies Inc. Deionized water (DI water) (>18 MΩ) was used in all aqueous solutions. Seawater used in electrochemical characterization were Zhuhai seawater.

Synthesis of $Co_3[Co(CN)_6]_2$ MOF (Co-PBA). The $Co_3[Co(CN)_6]_2$ MOF was synthesized by following methods: 1.40 g $CoCl_2 \cdot 6H_2O$ and 1.90 g $C_6H_9KO_7$ were dispersed in 100 mL of DI water. Then 1.30 g $K_3[Co(CN)_6]_2$ were dispersed in 100 mL of DI water and were added into above solution. After stirring for 8 h, the products were washed with DI water and collected by freeze-drying.

Synthesis of Ru_xCo-CN and Ru_xCo-CN-T. The as-prepared Co-PBA (60 mg) was dispersed in 30 ml deionized (DI) water under agitated stirring. Then 2 mL of freshly prepared $NaBH_4$ solution (1.0 mol L^{-1}) was injected into the above solution, then vigorous frothing occurs and the dark precipitate was observed immediately. The precipitate was filtered and washed several times with deionized water, and collected by freeze-drying. The precipitate was dispersed in 50 mL of DI water, followed by the addition of $RuCl_3$ solution (0.2 mol L^{-1}) with different atom ratios of Ru:Co (0.1,0.2, 0.3, 0.4, 0.5 and 0.6) to synthesis Ru_xCo-CN precursor. After agitated stirring for 8 h, the products were collected and rinsed several times by DI water, and finally dried under vacuum. The as-prepared precursor was annealed under high purity argon (Ar) at temperatures of 200 to 500 °C for 2 h with a heating rate of 5 °C min^{-1} to obtain the object Ru_xCo-CN-T products.

Synthesis of nano $Ru_{0.4}Co$ alloy. The nano $Ru_{0.4}Co$ alloy were synthesized by a hydrazine hydrate ($N_2H_4 \cdot H_2O$) reduction method.[1] For nano $Ru_{0.4}Co$, 0.4 mL of 0.2 M $RuCl_3$ and 1 mL of 0.1 M $CoCl_2 \cdot 6H_2O$ were dispersed in 7 mL of DI water, and then

0.33 mL of NaOH (20 M) and 1 mL of $N_2H_4 \cdot H_2O$ were added into the above solution. The resulting mixed solution was transferred to a Teflon-lined stainless-steel autoclave. After reaction at 180 °C for 3 h, the black products were obtained. The sample was washed with DI water, and collected by freeze-drying.

Materials Characterization. Scanning electron microscopy (SEM，HITACHI S-4800) operating at 5 kV, Transmission electron microscopy (TEM, JEOL JEM-2100 F), high-angle annular dark-field scanning TEM (HAADF-STEM) and energy-dispersive X-ray spectroscopy (EDS) analyses performed at 200 kV were used to investigate the morphology of samples. The crystallographic information was measured by X-ray diffraction (XRD, D8 ADVANCE X-ray diffractometer) patterns with Cu-Kα X-ray source (operating condition: 40 kV, 40 mA). X-ray photoelectron spectroscopy (XPS) measurements were carried out on ULVAC-PHI PHI Quantera II photoelectron spectroscope with Al-Kα excitation source, and all spectra were calibrated to a C 1s peak position of 284.8 eV. Thermogravimetric and differential scanning calorimetry analysis (TG-DSC) were measured by NETZSCH STA 449 F3 thermogravimetric analyzer with a heating rate of 10 °C min^{-1} under Ar atmosphere. Fourier transform infrared (FT-IR) spectra were recorded using a Nicolet Avatar 360 FT-IR infrared spectrometer with a Bruker VerTex 80v spectrometer. Raman spectra were conducted on a Renishaw InVia Raman spectrometer under visible excitation at 532 nm. The metal contents of the sample or in electrolyte was measured by inductively-coupled plasma-atomic emission spectroscopy (ICP-AES, LEEMAN LABS Prodigy7).

Electrochemical Characterization. Electrochemical experiments were performed in Autolab PGSTAT30 and Corrtest CS350M working station with a three-electrode system. The electrochemical experiments were carried out in electrolyte with different pH values: 1.0 mol L^{-1} KOH + 3.5% wt. NaCl ("alkaline sS", pH = 14), 1 mol L^{-1} KOH + natural seawater ("alkaline nS", pH = 14), 1 mol L^{-1} PBS buffer + 3.5% wt. NaCl ("neutral sS", pH = 7), 1 mol L^{-1} PBS buffer + natural seawater ("neutral nS", pH = 7), 0.5 mol L^{-1} H_2SO_4 + 3.5% wt. NaCl ("acidic sS", pH = 0) and 0.5 mol L^{-1} H_2SO_4 + natural seawater ("acidic nS", pH = 0). The alkaline simulated seawater was prepared by adding NaCl with mass fraction of 3.5 % to the as prepared KOH solution, which is

close to the artificial seawater.[1-4] The natural seawater is taken from Zhuhai. For electrolyzer, a catalyst-supported glassy-carbon rotating disk electrode (RDE, diameter of 0.5 cm and geometric area of 0.196 cm^2) was used as the working electrode, an Ag/AgCl electrode filling with saturated solution of KCl was employed as the reference electrode in simulated seawater electrolyte, and a reversible hydrogen electrode was used as the reference electrode in the KOH electrolyte. For the catalyst inks, 5.0 mg of the catalyst powder and 50 μL 5% Nafion was added into 950 μL isopropyl alcohol, followed by ultrasonication in an ice-bath for 30 min. The average mass loading of RDE was 0.255 mg cm^{-2} and the catalyst loading on Ni foam (NF) and carbon cloth (CC) is 1.0 mg cm^{-2} followed by drying at 60 °C for at least 12 h. The RDE is measured under a spin of 1600 rpm, the catalyst is easily to be shed during the long-time stability tests and the mass bubble can heighten this process, which will reduce the performance of catalyst. As a result, the stability of catalysts tested on RDE are poor than they loaded on NF and CC.

Before the tests, the electrolyte would be saturated with nitrogen and all the measurements were under nitrogen flow. The working electrode was activated by cyclic voltammetry (CV) test with the scan rate of 100 mV s^{-1} between -0.2 to 0.05 V (vs. RHE, HER) and 1.2 to 1.63 V (vs. RHE, OER) for 20 cycles before performance test, and the linear sweep voltammetry (LSV) measurements were performed at the scan rate of 5 mV s^{-1} and were corrected by the iR loss. All measured potentials were calibrated to the reversible hydrogen electrode (RHE), with the equation: E vs.RHE = Evs.Ag/AgCl + 0.197 V + 0.0592 V × pH. The electrochemical impedance spectroscopy (EIS) tests were performed at the overpotential of 10 mV over the frequency range of 100 kHz to 0.005 Hz and a small sine-wave distortion (AC signal) of 10 mV amplitude. Electrochemical double layer capacitor (C_{dl}) was derived from double-layer charging curves using CV sweep with scan rate from 20 to 100 mV s^{-1}.

For overall seawater splitting device, a two-electrode cell was assembled by two identical $Ru_{0.4}$Co-CN-T electrodes carried by NF and CC for stability tests. After activated by CV tests, the stability measurements were conducted by chrono-potentiometric measurements and applying constant current. The solar cell

electrocatalytic seawater splitting device was assembled by two $Ru_{0.4}Co$-CN-T electrodes in a H-type electrolytic cell, driven by a commercial silicon solar cell with simulated solar irradiation. The amount of collected H_2 and O_2 gases were calculated by the drainage method and were used to calculate the Faradaic efficiency. The iR compensation was not applied in overall seawater water splitting measurements.
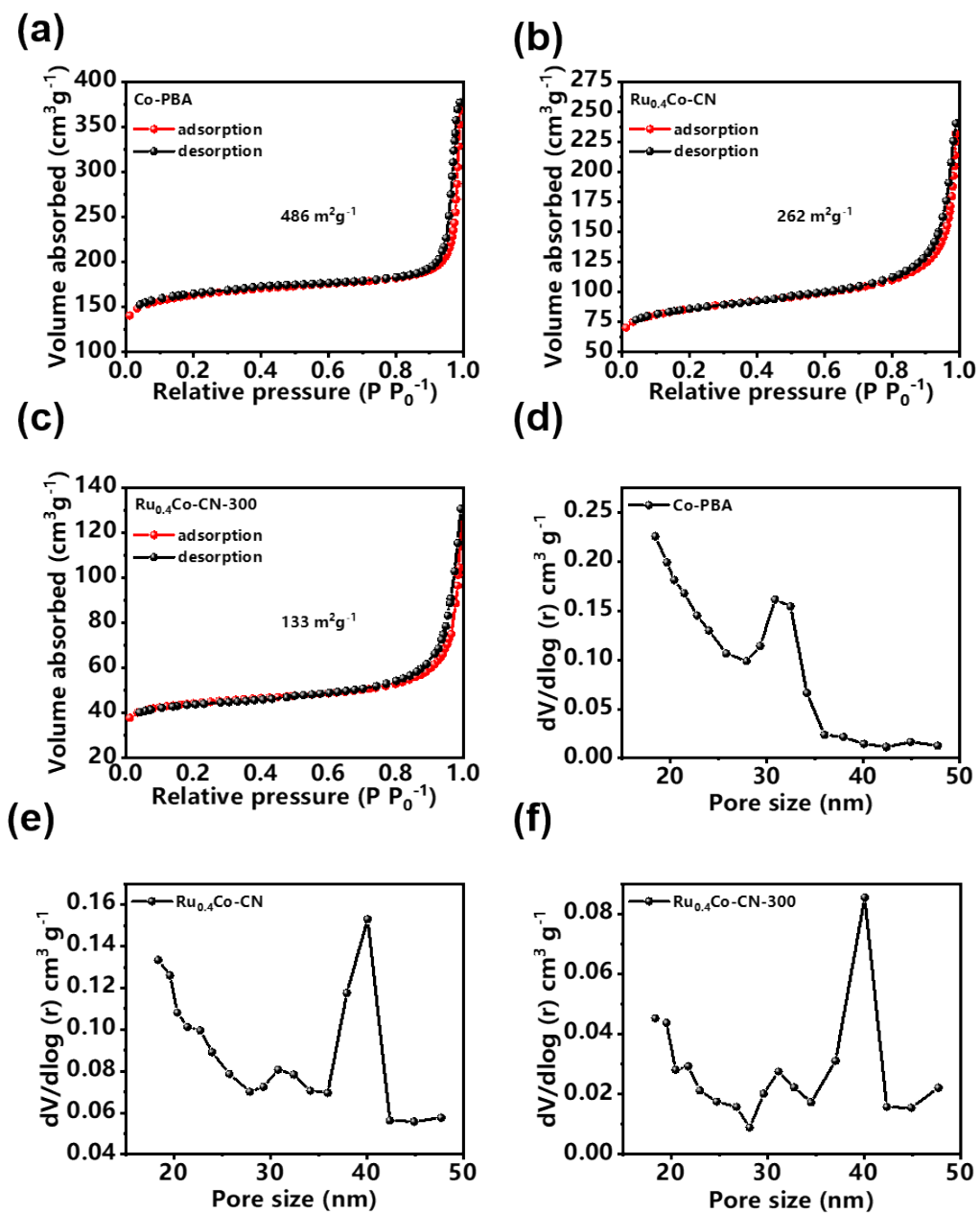
Figure S1. (a-c) The N_2 adsorption-desorption isotherms and (d-f) corresponding pore size distribution of Co-PBA, $Ru_{0.4}Co$-CN and $Ru_{0.4}Co$-CN-300.

Table S1. The content of Co and Ru in $Ru_{0.4}Co$-CN and $Ru_{0.4}Co$-CN-300 detected by inductively coupled plasma-atomic emission spectroscopy (ICP-AES).

	Co content (at. %)	Ru content (at. %)
$Ru_{0.4}Co$-CN	61.3	38.7
$Ru_{0.4}Co$-CN-300	62.1	37.9

Based on Table S1, the actual Ru/Co molar ratio is about 0.4, which are consistent with the molar ratios of $RuCl_3$: Co-PBA in experiment. However, atomic ratios of Ru: Co in alloy are hard to be obtained due to the metal oxides formed in these samples.
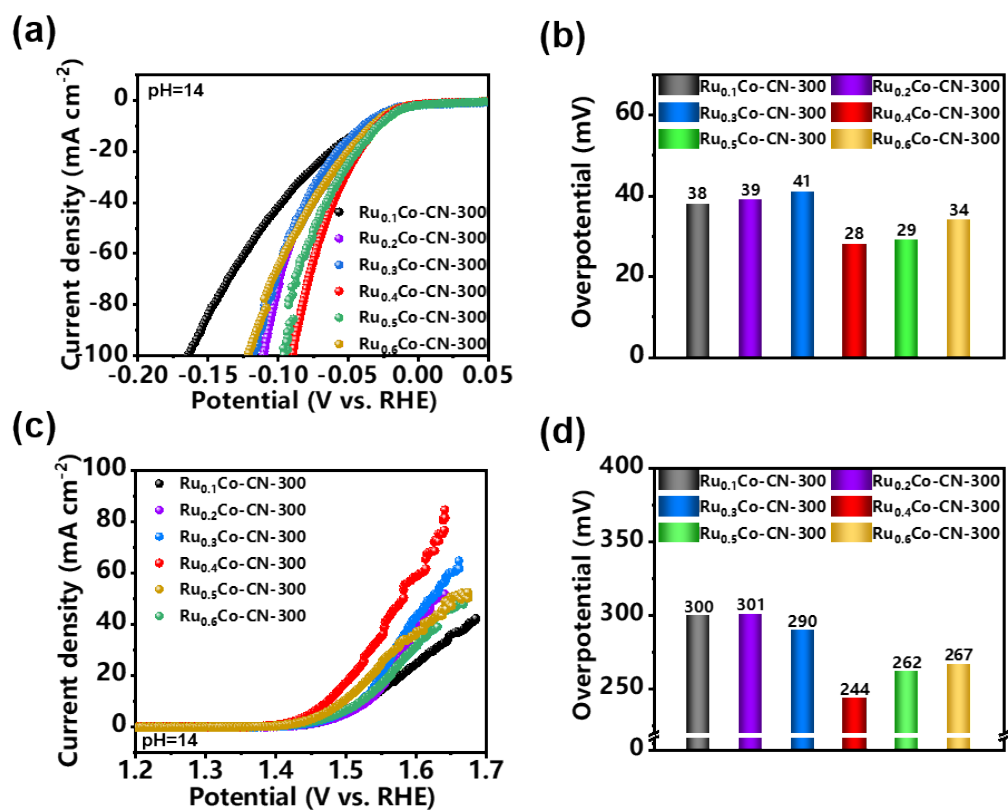
Figure S2. HER and OER performances of $Ru_{0.1}$Co-CN-300, $Ru_{0.2}$Co-CN-300, $Ru_{0.3}$Co-CN-300, $Ru_{0.4}$Co-CN-300, $Ru_{0.5}$Co-CN-300 and $Ru_{0.6}$Co-CN-300 in alkaline seawater. (a) HER polarization curves, (b) Comparison of HER overpotential @10 mA cm^{-2}, (c) OER Polarization curves and (d) Comparison of OER overpotential @10 mA cm^{-2}.

$Ru_{0.4}$Co-CN-300 (Ru:Co ratio of 0.4 determined by ICP-AES, Table S1) display the best electrocatalytic performance in alkaline seawater and was used for further study.
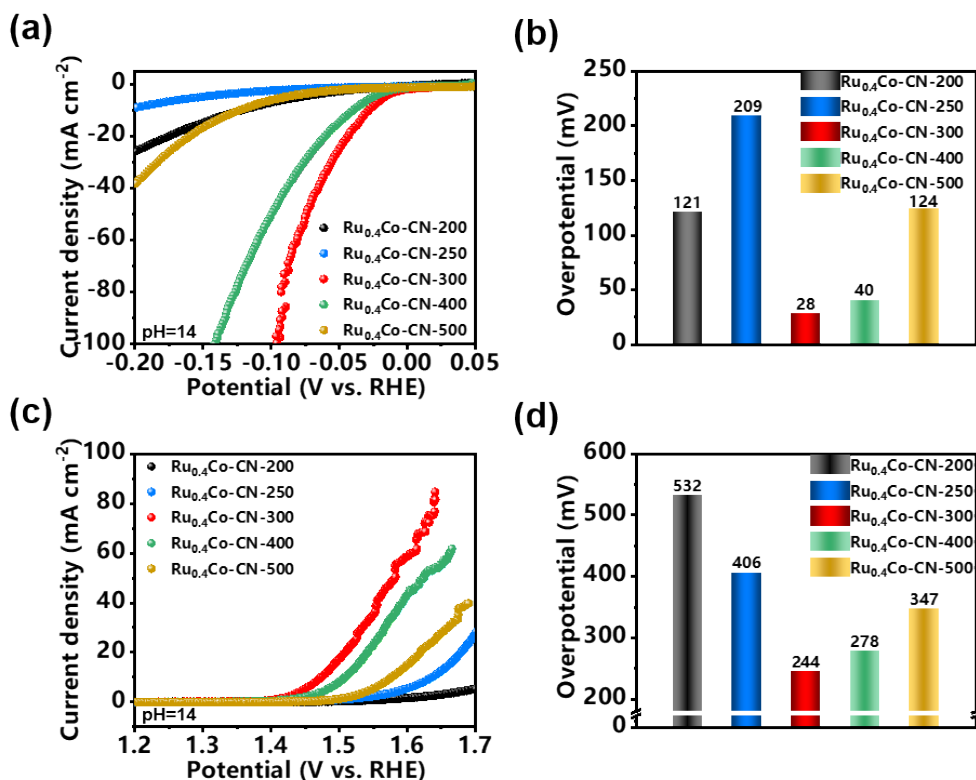
Figure S3. HER and OER performance of $Ru_{0.4}Co$-CN-200, $Ru_{0.4}Co$-CN-250, $Ru_{0.4}Co$-CN-300, $Ru_{0.4}Co$-CN-400 and $Ru_{0.4}Co$-CN-500 in alkaline seawater. (a) HER polarization curves, (b) Comparison of HER overpotential @10 mA cm^{-2}, (c) OER Polarization curves and (d) Comparison of OER overpotential @10 mA cm^{-2}.
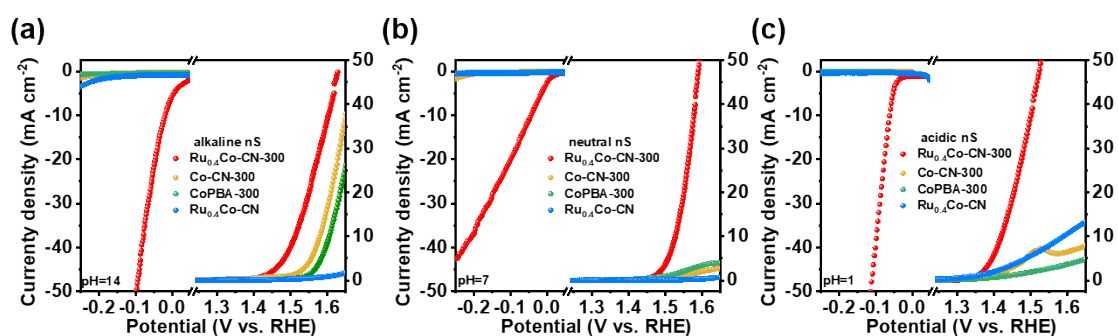
Figure S4. HER and OER performance of $Ru_{0.4}Co$-CN-300, Co-CN-300, CoPBA-300, and $Ru_{0.4}Co$-CN in different media. (a) alkaline seawater, (b) neutral seawater and (c) acidic seawater
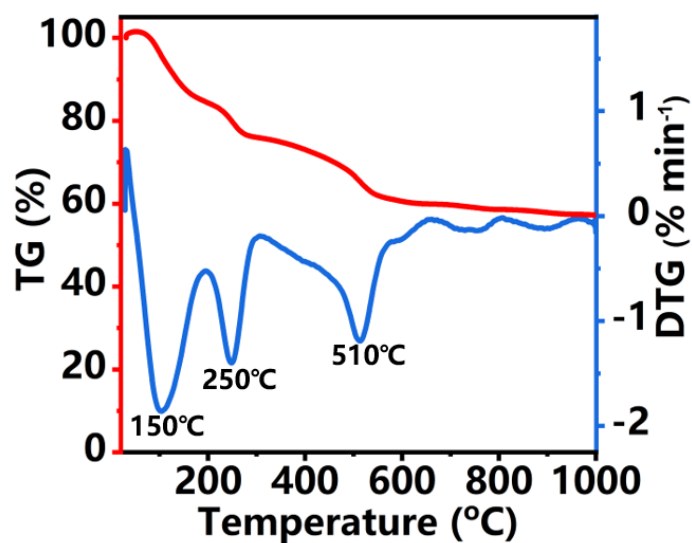
Figure S5. TG-DSC analysis of $Ru_{0.4}Co$-CN precursor, in argon.
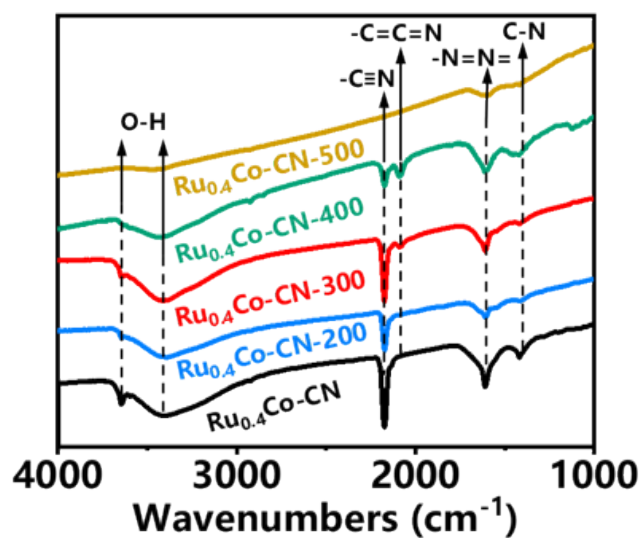
Figure S6. FT-IR spectra of the $Ru_{0.4}Co$-CN, $Ru_{0.4}Co$-CN -200, $Ru_{0.4}Co$-CN-300, $Ru_{0.4}Co$-CN-400 and $Ru_{0.4}Co$-CN-500 respectively.
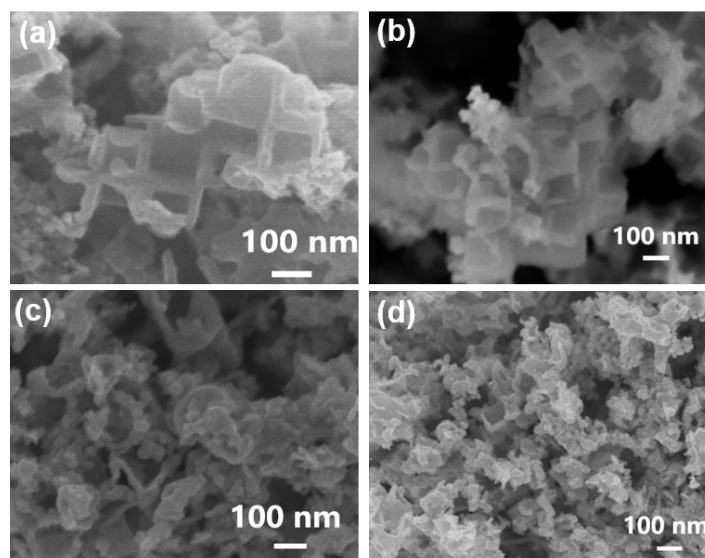
Figure S7. SEM images of (a) $Ru_{0.4}Co$-CN-200, (b) $Ru_{0.4}Co$-CN-300, (c) $Ru_{0.4}Co$-CN-400 and (d) $Ru_{0.4}Co$-CN-500.
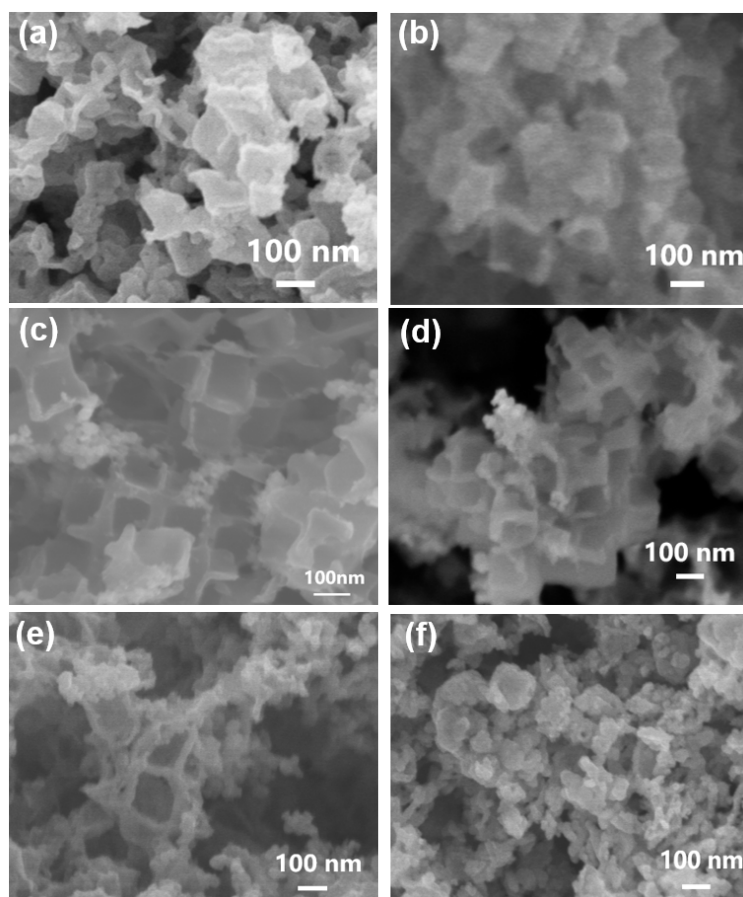
Figure S8. SEM images of (a) $Ru_{0.1}Co$-CN-300, (b) $Ru_{0.2}Co$-CN-300, (c) $Ru_{0.3}Co$-CN-300, (d) $Ru_{0.4}Co$-CN-300, (e) $Ru_{0.5}Co$-CN-300 and (f) $Ru_{0.6}Co$-CN-300.
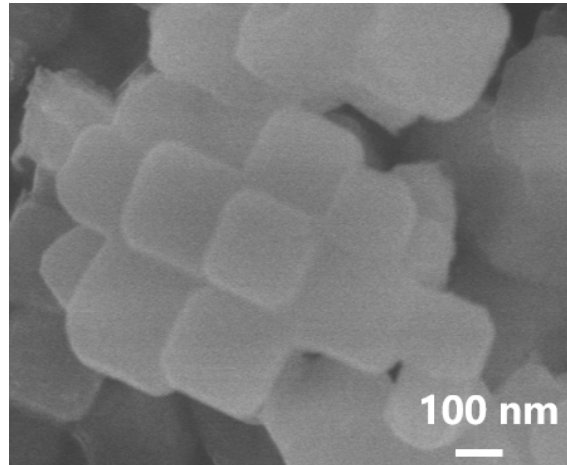
Figure S9. SEM images of Co-PBA.
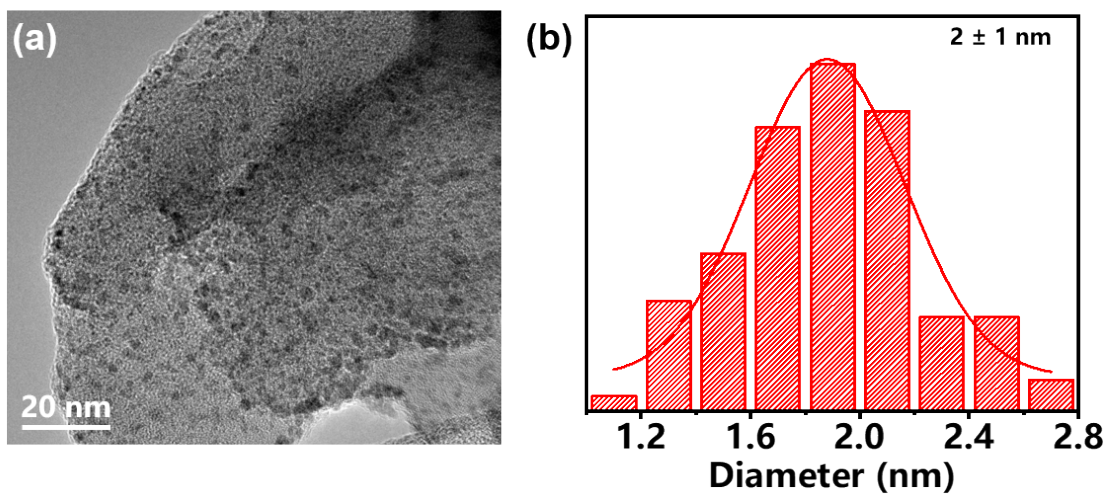
Figure S10. (a) TEM images and (b) histogram of the diameters of Ru-Co nanoparticles for $Ru_{0.4}Co$-CN-300.
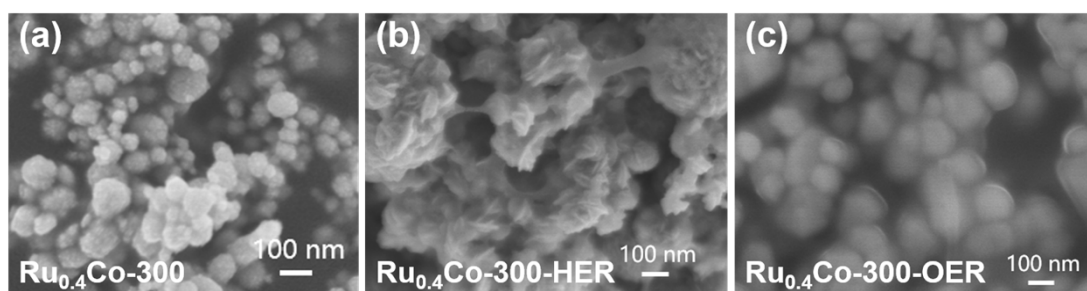
Figure S11. SEM images of (a) $Ru_{0.4}Co$-300, (b) $Ru_{0.4}Co$-300 after HER tests and (c) $Ru_{0.4}Co$-300 after OER tests.

The structure of $Ru_{0.4}Co$-300 is agglomerated nanoparticle and adverse to exposure of reactive sites, finally leading to a low catalytic activity.
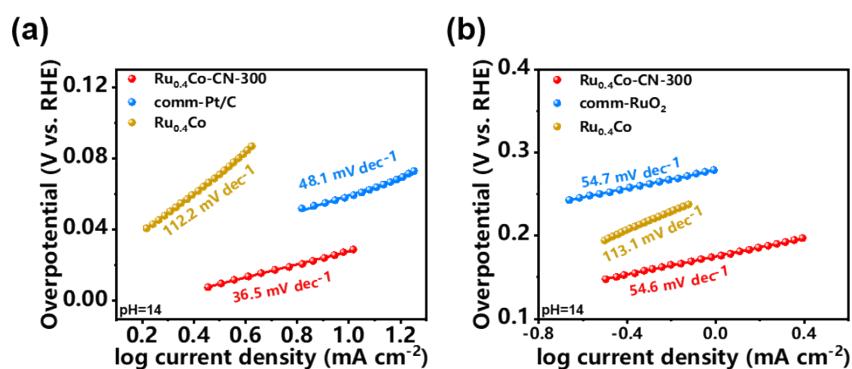

Figure S12. Tafel slopes of $Ru_{0.4}Co$-CN-300, commercial Pt/C, commercial RuO_2 and $Ru_{0.4}Co$ alloy. (a) HER and (b) OER in alkaline simulate seawater.
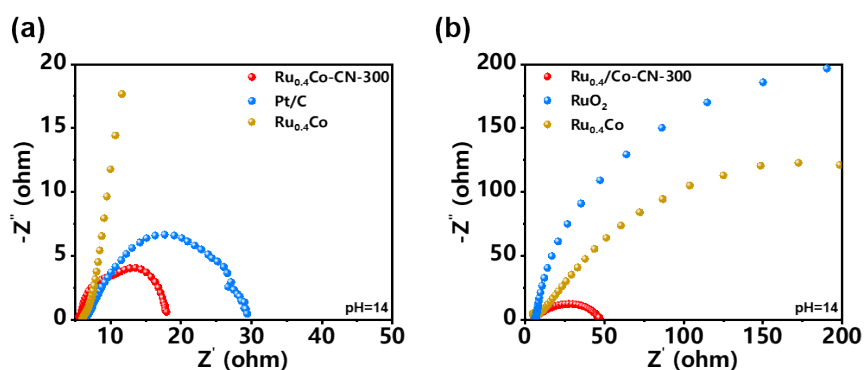

Figure S13. Nyquist plots of $Ru_{0.4}Co$-CN-300, commercial Pt/C, commercial RuO_2 and $Ru_{0.4}Co$ alloy. (a) HER and (b) OER.
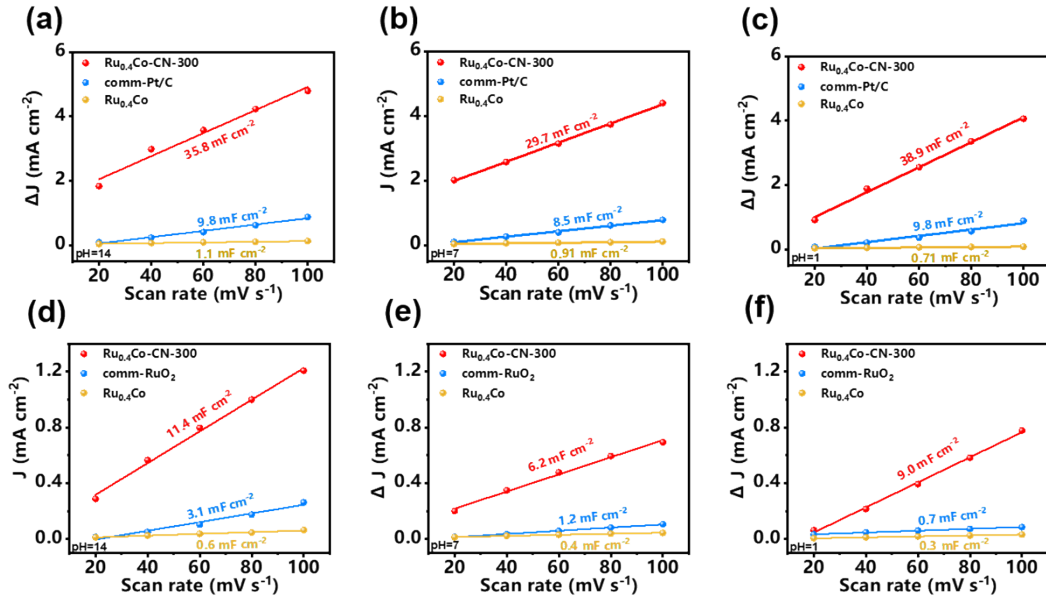
Figure S14. Electrochemical double-layer capacitance of $Ru_{0.4}Co$-CN-300, commercial Pt/C, commercial RuO_2 and $Ru_{0.4}Co$ alloy in alkaline, neutral and acidic seawater. (a-c) HER between 0.1 to 0.2 V (vs. RHE) and (d-f) OER between 1.2 to 1.3 V (vs. RHE).
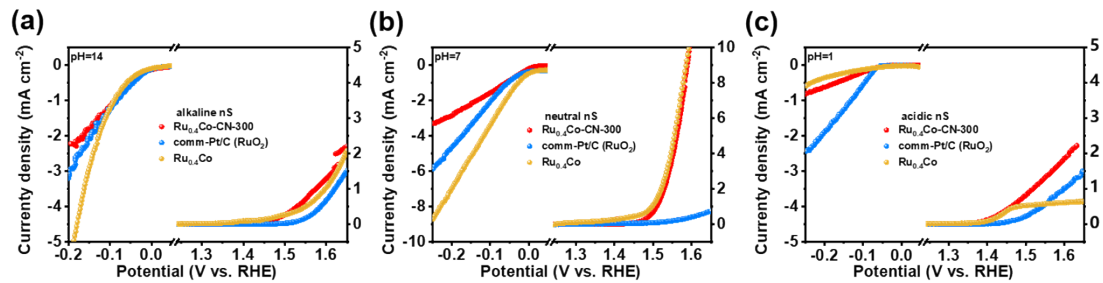

Figure S15. polarization curves normalized by ECSA of $Ru_{0.4}Co$-CN-300, commercial Pt/C, commercial RuO_2 and $Ru_{0.4}Co$ alloy in alkaline, neutral and acidic seawater.

For the calculation of electrochemical active surface area (ECSA), the value of specific capacitance (C_s) for a flat surface (1 cm^{-2}) is respectively assumed as 40 $\mu F\ cm^{-2}$, 120 $\mu F\ cm^{-2}$ and 20 $\mu F\ cm^{-2}$ under pH conditions of 14, 7 and 1. The ECSA is calculated according to the following equation: ECSA = C_{dl} / C_s. Results indicate that the large number of Ru-Co alloy active sites on the surface of N-doped carbon cages play an important role in the outstanding catalytic performance of $Ru_{0.4}Co$-CN-300.

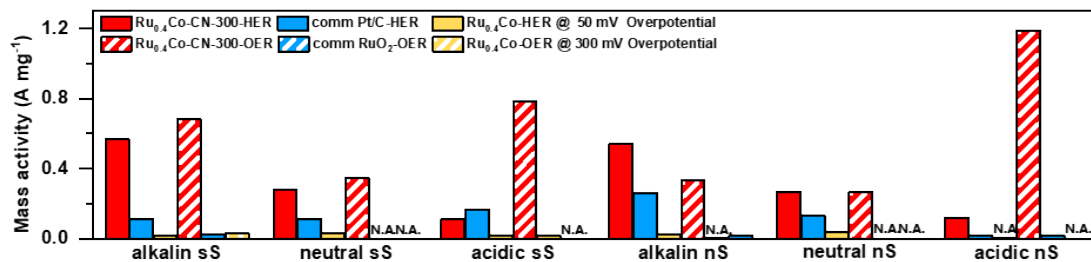**Figure S16.** Comparison of mass activity of $Ru_{0.4}Co$-CN-300, commercial Pt/C, commercial RuO_2 and $Ru_{0.4}Co$ alloy at a given HER overpotential of 50 mV and OER overpotential of 300 mV in different conditions.

The loading masses of $Ru_{0.4}Co$-CN-300, commercial Pt/C, commercial RuO_2 and $Ru_{0.4}Co$ alloy were calculated to be around 0.04, 0.05, 0.19 and 0.10 mg cm^{-2}. The mass activity at a given HER overpotential of 50 mV and OER overpotential of 300 mV in different conditions had been compared and $Ru_{0.4}Co$-CN-300 shows best performance, indicating that the mass activity of $Ru_{0.4}Co$-CN-300 is the highest.
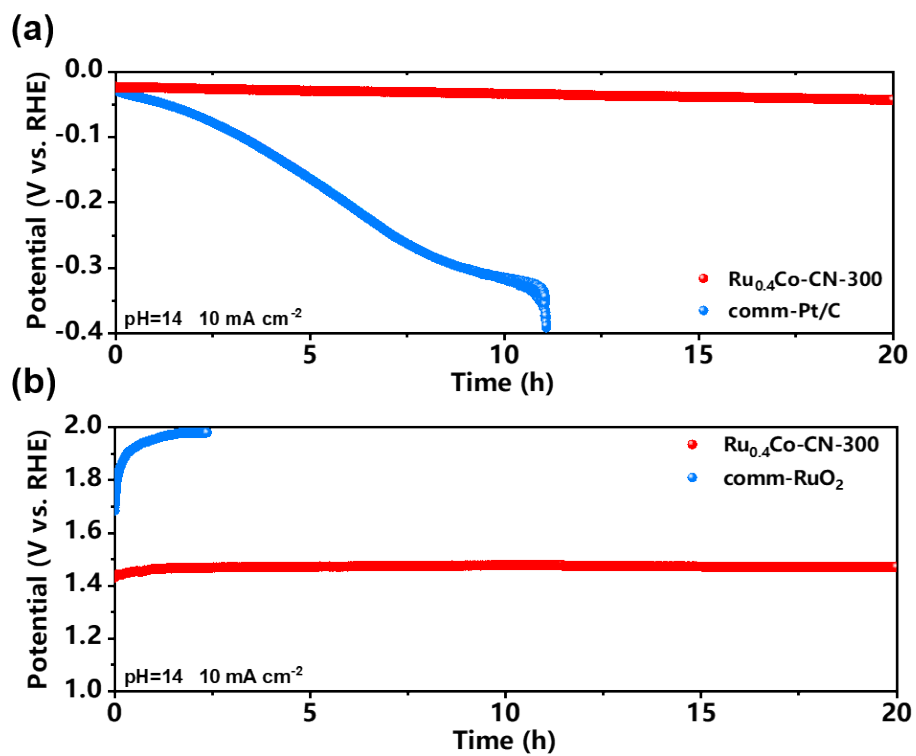
Figure S17. Chronoamperometric tests of Ru$_{0.4}$Co-CN-300, commercial Pt/C and commercial RuO$_2$ at the current density of 10 mA cm^{-2} in alkaline seawater. (a) HER and (b) OER.
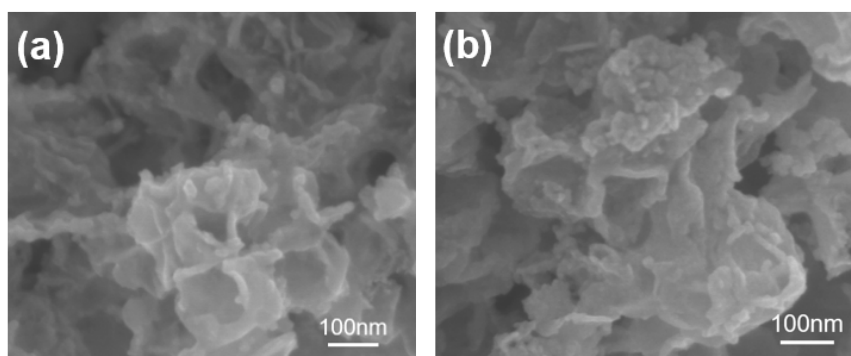
Figure S18. SEM images of $Ru_{0.4}Co$-CN-300 electrode after stability tests in alkaline seawater: (a) after HER and (b) after OER.
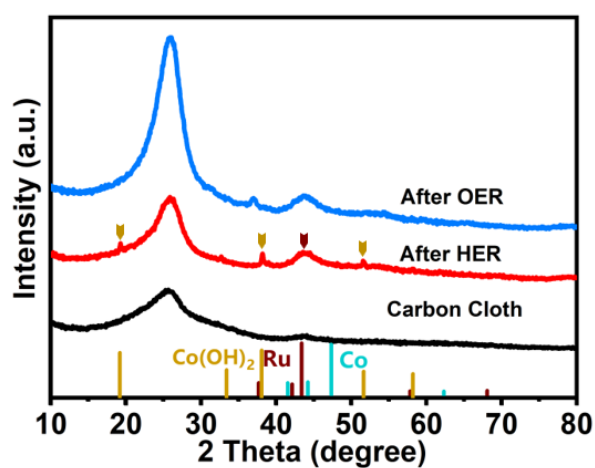

Figure S19. XRD patterns of $Ru_{0.4}Co$-CN-300 and electrode of $Ru_{0.4}Co$-CN-300 after HER and OER tests in alkaline seawater.
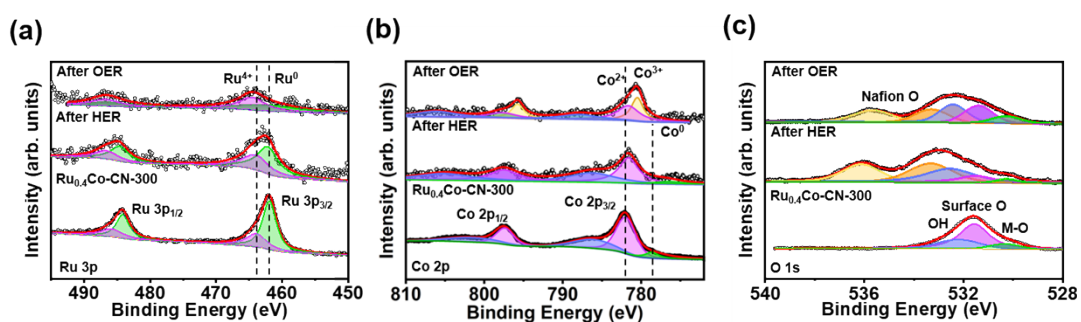
Figure S20. XPS spectra for Ru$_{0.4}$Co-CN-300 and electrode of Ru$_{0.4}$Co-CN-300 after HER and OER tests in alkaline seawater: (a) Ru 3p, (b) Co 2p and (c) O 1s.
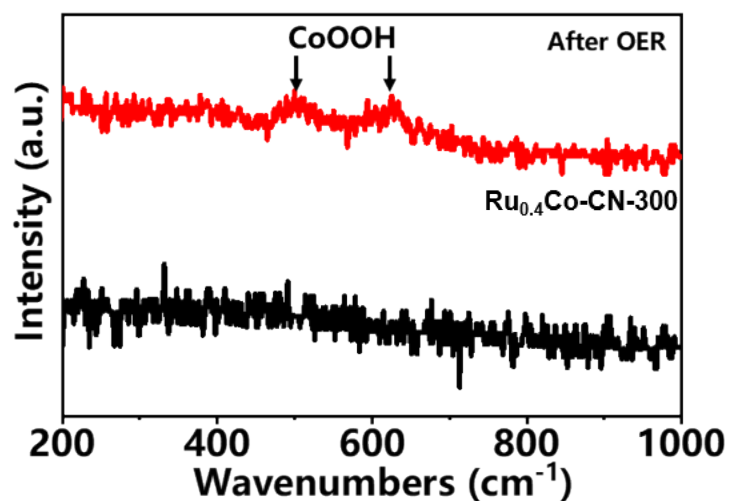

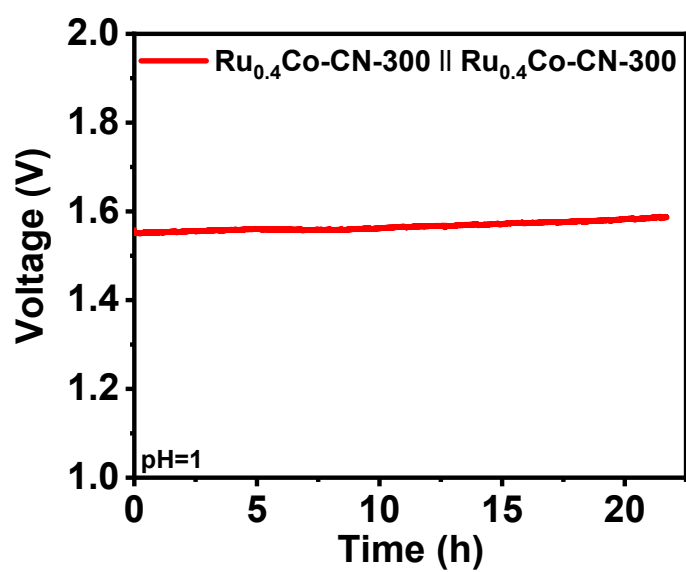**Figure S21.** Raman spectroscopy for Ru$_{0.4}$Co-CN-300 and electrode of Ru$_{0.4}$Co-CN-300 after OER tests.

Figure S22. Chronoamperometric tests of $Ru_{0.4}Co$-CN-300 $\|$ $Ru_{0.4}Co$-CN-300 in acidic seawater.
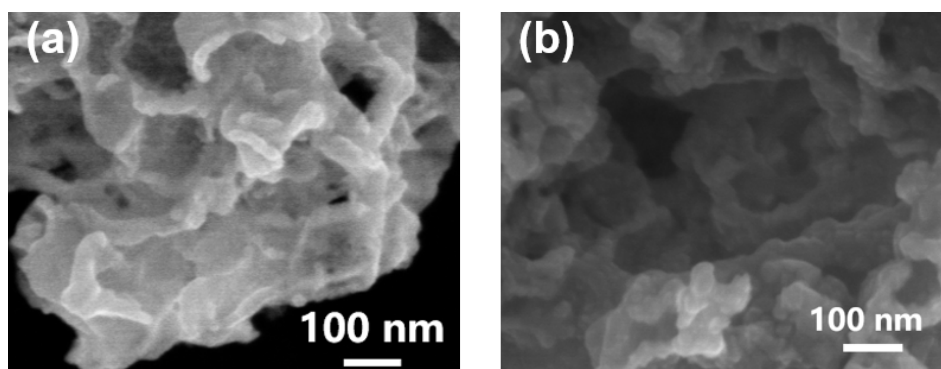

Figure S23. SEM images of $Ru_{0.4}Co$-CN-300 electrode after stability tests in acidic seawater: (a) after HER and (b) after OER.
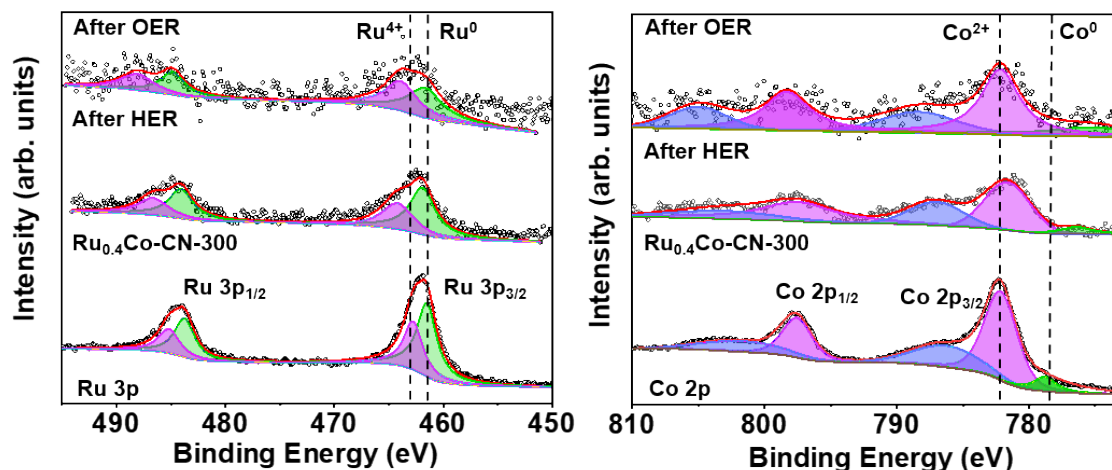
Figure S24. XPS spectra for Ru$_{0.4}$Co-CN-300 and electrode of Ru$_{0.4}$Co-CN-300 after HER and OER tests in acidic seawater: (a) Ru 3p and (b) Co 2p.

According to the XPS spectra, the peaks of Ru^{4+} and Ru^0 can be detected and the ratio of Ru^{4+} is higher after OER stability test. While only the peaks of Co^{2+} are retained after the reactions. The results indicate that some ruthenium oxide formed on the surface after OER and metallic Co resolved in acidic electrolyte. The etched Ru-Co alloy contain favorable performance and stability for HER in acidic electrolyte. The ruthenium oxide mixed with etched Ru-Co alloy are contributed to OER activity.
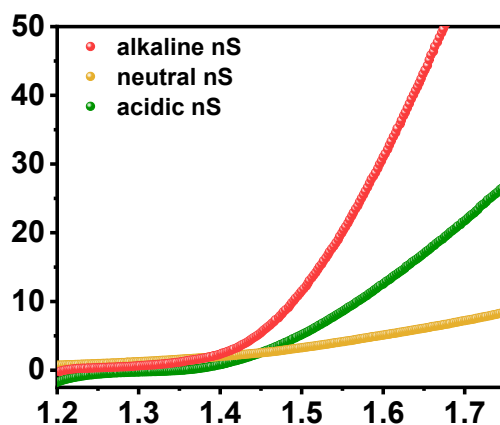
Figure S25. Overall seawater splitting polarization curves of $Ru_{0.4}Co$-CN-300 $\|$ $Ru_{0.4}Co$-CN-300 in alkaline, neutral and acidic nature seawater.
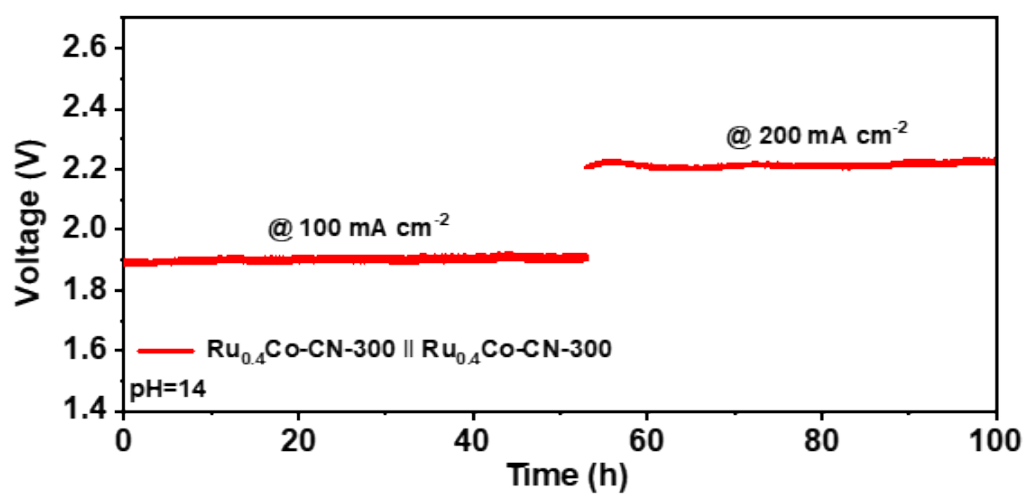
Figure S26. Chronoamperometric tests of $Ru_{0.4}Co$-CN-300 $\|$ $Ru_{0.4}Co$-CN-300 at the current density of 100 mA cm^{-2} and 200 mA cm^{-2} in alkaline seawater.
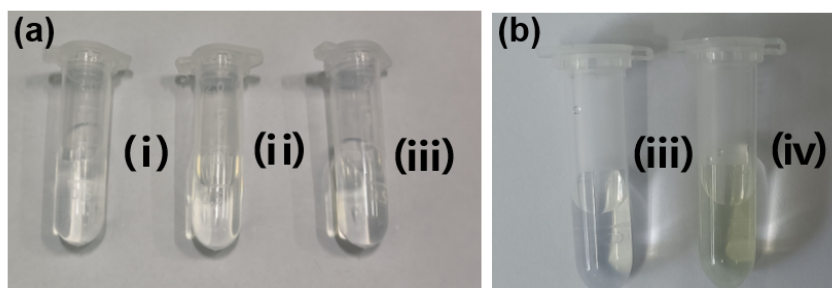
Figure S27. Digital graphs of the corresponding mixed solutions for (a) $Ru_{0.4}Co$-CN-300 (i) after 10 mA cm^{-2} (ii) after 50 mA cm^{-2} (iii) after 100 mA cm^{-2} and (b) $Ru_{0.4}Co$-CN-300 after 100 mA cm^{-2} and (iv) Pt/ClIRuO$_2$ after 100 mA cm^{-2}.

O-Tolidine test was used to detect whether the ClO$^-$ formed during the seawater splitting tests. In Figure S18, the color of mixed solutions for $Ru_{0.4}Co$-CN-300 electrolyte after 300 hours seawater splitting are colorless and no characteristic adsorption peaks were observed in the UV−vis spectrum, indicating that there are no ClO$^-$ formed. However, the color of mixed solution for Pt/ClIRuO$_2$ turned into yellow and there is obvious absorption peak around 437 nm, confirmed the formation of ClO$^-$.
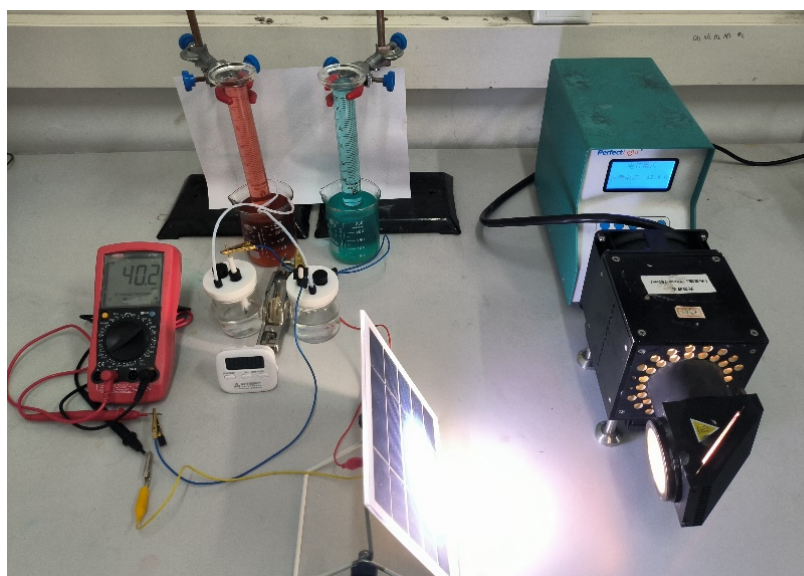

Figure S28. A photo of solar-driven overall seawater splitting device based on $Ru_{0.4}Co$-CN-300 (1 cm^2 electrodes) and commercial Si solar cell.

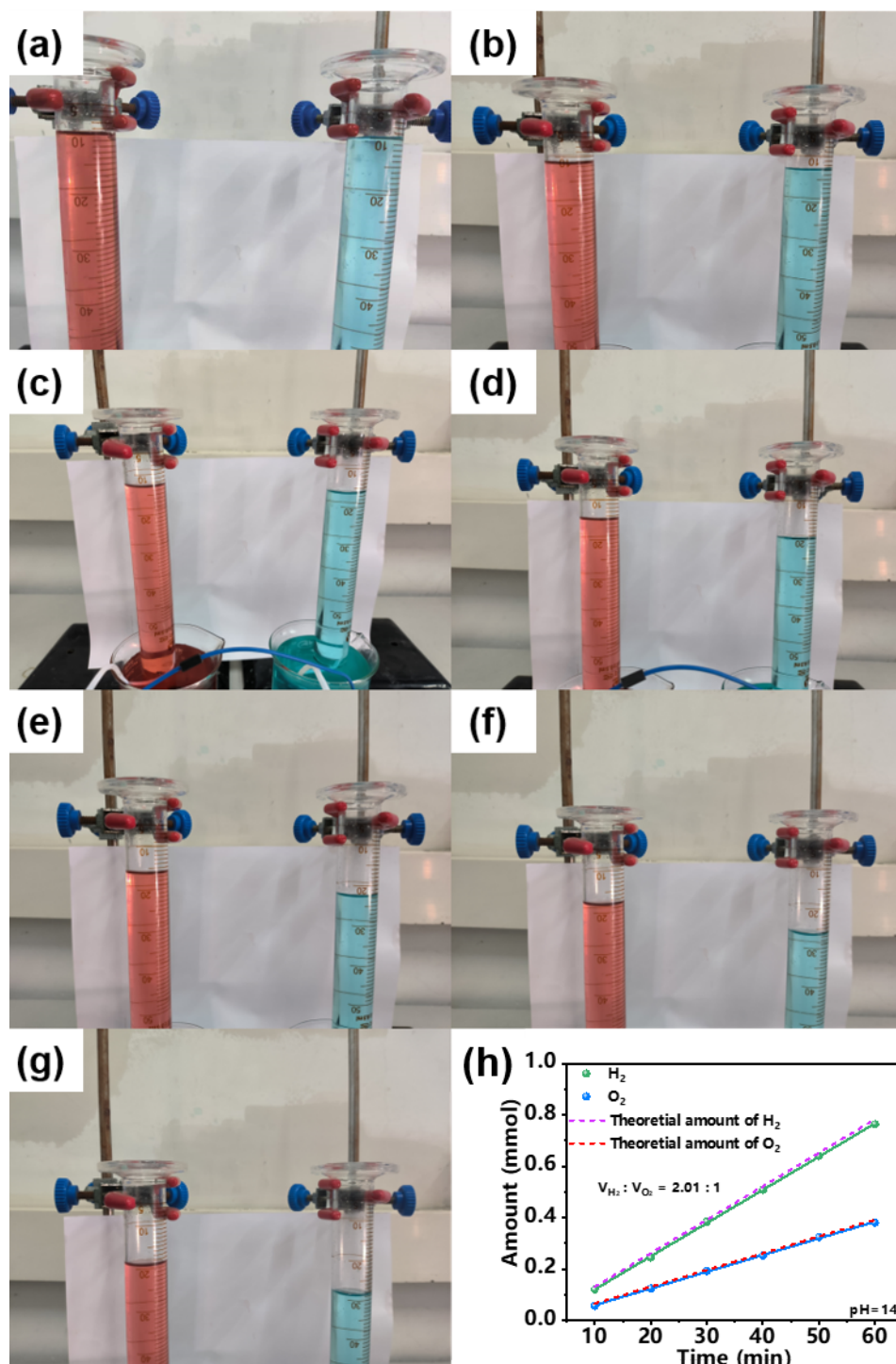**Figur**e **S29.** (a-g) Photographs of collected H_2 and O_2 at different time and (h) volume of collected H_2 and O_2 for $Ru_{0.4}Co$-CN-300 catalyst versus time.

Table S2. The amount of collected H_2 and O_2 gases.

	10 min	20 min	30 min	40 min	50 min	60 min
H_2 (mL)	3	6.1	9.6	12.7	16	19.1
H_2 (mmoL)	0.12	0.24	0.38	0.51	0.64	0.76
O_2 (mL)	1.4	3.1	4.8	6.3	8.1	9.5
H_2 (mmoL)	0.056	0.124	0.192	0.252	0.324	0.38

The Faradaic efficiency of H_2 is calculated by dividing the amount of H_2 gas collected experimentally by the theoretical hydrogen production calculated using the amount of charge. The current density is 42 mA cm^{-2} (area of electrode: 1 cm^2) during the alkaline seawater electrolysis. Faradaic efficiency (H_2) = n × (collected H_2) × 2 / n(electron) × 100% = 0.920 × 2 × 10^{-3} mol / (0.05 A × 3600 s / 96485 C mol^{-1}) × 100%= 97.5%. The Faradaic efficiency of O_2 is calculated to be ~97.1% by the same method.

Table S3. Comparison of HER and OER performances for $Ru_{0.4}Co$-CN-300 with other reported electrocatalysts in alkaline media.

	η@j (mV @mA cm^{-2})	Ref
$Ru_{0.4}Co$-CN-300	**28@10 (HER)** **244@10 (OER)**	**This work**
NiFeRu/C	55@10 (HER) 249@10 (OER)	*J. Colloid Interface Sci.* **2023**, *651*, 1008–1019
$Co(Ni)O_x$	97@10 (HER) 319@10 (OER)	*Appl. Mater.* **2023**, *34*, 101912
Ru-FeNi	39@10 (HER) 198@10 (OER)	*Angew. Chem. Int. Ed.* **2023**, *62*, e202306333
$CoFe_2O_4$	106@10 (HER) 162@10 (OER)	*J. Alloys Compd.* **2022**, *895*, 162614
$Ru–NiSe_2$	59@10 (HER) 210@10 (OER)	*Small* **2022**, *18*, 2105305
Fe-Co_2P	73@10 (HER) 210@10 (OER)	*Catalysts* **2022**, *12*, 957
$RuCoO_x$	73@10 (HER) 210@10 (OER)	*Chem. Asian. J.* **2021**, *16*, 2511-2519
Na-Ru	30@10 (HER) 174@10 (OER)	*Adv. Funct. Mater.* **2021**, *31*, 2010437
Ru-CoMo	56@10 (HER) 237@10 (OER)	*Appl. Surf. Sci.* **2021**, *541*, 148518
Ru-$Co(OH)_2$	55@10 (HER) 295@10 (OER)	*J. Taiwan Inst. Chem. Eng.* **2020**, *109*, 71-78
Ru-Co@CDs	51@10 (HER) 257@10 (OER)	*J. Mater. Chem. A* **2020**, *8*, 9638
RuCu NSs	20 @10 (HER) 234 @10 (OER)	*Angew. Chem.* **2019**, *131*, 14121-14126
CF–NG–Co	20@10 (HER) 367@10 (OER)	*J. Mater. Chem. A* **2018**, *6*, 489

References

1. D. R. Kester, I. W. Duedall, D. N. Connors and R. M., *Limnol. Oceanogr.*, 2003, **12**, 176-179.
2. F. J. Millero, R. Feistel, D. G. Wright and T. J. McDougall, *DEEP-SEA RES. PT. I*, 2008, **55**, 50-72.
3. H. Zou, X. Meng, X. Zhao and J. Qiu, *Adv. Mater.*, 2023, **35**, 2207262.
4. M. Wang, P. Zhang, X. Liang, J. Zhao, Y. Liu, Y. Cao, H. Wang, Y. Chen, Z. Zhang, F. Pan, Z. Zhang and Z. Jiang, *Nat. Sustain.*, 2022, **5**, 518-526.